A Wideband 3D Printed Reflectarray Antenna with Mechanically Reconfigurable Polarization

Mei, Peng; Zhang, Shuai; Pedersen, Gert Frølund

Published in:
I E E E Antennas and Wireless Propagation Letters

DOI (link to publication from Publisher):
10.1109/LAWP.2020.3018589

Publication date:
2020

Document Version
Accepted author manuscript, peer reviewed version

Citation for published version (APA):
Mei, P., Zhang, S., & Pedersen, G. F. (2020). A Wideband 3D Printed Reflectarray Antenna with Mechanically Reconfigurable Polarization. *I E E E Antennas and Wireless Propagation Letters*, *19*(10), 1798-1802. Article 9173781. https://doi.org/10.1109/LAWP.2020.3018589

A Wideband 3D Printed Reflectarray Antenna with Mechanically Reconfigurable Polarization

Peng Mei, *Student Member, IEEE*, Shuai Zhang, *Senior Member, IEEE*, and Gert Frølund Pedersen, *Member, IEEE*

***Abstract*—This letter describes a wideband and polarization-reconfigurable reflectarray (RA) antenna using 3D printed technology for 5G millimeter-wave applications. An air-perforated dielectric stub is proposed as a unit cell (UC) to provide simultaneous polarization-rotation and phase-shifting capabilities. By optimizing the dimensions of the UC, four UCs are found to offer a 90-degree out of phase for transverse electric (TE) and transverse magnetic (TM) incidence waves and a 2-bit reflection phase of {-π, -π/2, 0, π/2}, which are employed to implement the reflective panel. By rotating the reflective panel mechanically, the proposed RA antenna can achieve linear polarization (LP), left-hand circular polarization (LHCP), and right-hand circular polarization (RHCP) modes. The measured results are highly consistent with the simulated counterparts, indicating that the proposed RA antenna can reach a 3-dB axial ratio (AR) bandwidth of 43.2 %, and 37.5 % for RHCP and LHCP modes, respectively. Besides, a 3-dB gain bandwidth of 37.5 %, 34.4 %, and 37.5 % is experimentally obtained for RHCP, LHCP, and LP modes of the proposed RA antenna, respectively.**

***Index Terms*— High-gain, polarization-agility, wideband, 3D printed technology, low-cost, 5G millimeter-wave.**

I. Introduction

Polarization-reconfigurable antennas play important roles in wireless communication systems [1]-[3]. Lots of efforts have been dedicated to improving the performance of such antennas [4]-[16]. One of the popular techniques to achieve polarization agility is to design a radiator loading with PIN diodes [4]-[8], where the radiator can work in a linearly or circularly-polarized manner by controlling the bias voltages. In [6], the authors proposed a reconfigurable corner-truncated patch loading with four PIN diodes to achieve linear polarization (LP), left-hand circular polarization (LHCP), and right-hand circular polarization (RHCP), resulting in a 3-dB axial ratio (AR) bandwidth of 1.5 % for LHCP and RHCP modes. Another widely-used one is to use reconfigurable feeding networks [9]-[14]. The authors in [13] designed a microstrip-slot line-coplanar waveguide feed network loading with three PIN diodes to generate LP, LHCP, and RHCP modes by manipulating the bias voltages, where a 3-dB AR bandwidth of 14.5 % and 15.0 % is obtained for LHCP and RHCP modes, respectively. The polarization agility of reconfigurable antenna can also be obtained by mechanically rotating the metasurface or superstrate above a slot planar antenna [15] or a L-probe feed [16]. The mechanical control has its unique superiorities of low loss and simple structures.

In this paper, a wideband and polarization-reconfigurable reflectarray antenna based on 3D printed technology is proposed for 5G millimeter-wave wireless communications. On one hand, reflectarray antennas can offer high gains without using complicated feeding networks, and are found to achieve reconfigurable beams by controlling the reflection phases of unit cells of the reflectarray [17]-[19]. On the other hand, 3D printed technologies have attracted much attention due to their feasibilities and advantages in antenna manufacturings. Lots of 3D printed antennas have been reported to demonstrate high-gain, low-cost, wideband, and other attractive properties in the millimeter-wave and terahertz frequency bands [20]-[23]. To construct the proposed RA antenna, a dielectric stub with a cuboid-shaped air void is proposed as a unit cell (UC) for the reflective panel implementation. To simplify the proposed RA antenna design, four UCs are optimized to provide a 2-bit reflection phase of {-π, -π/2, 0, π/2} and a 90-degree out of phase for TE and TM incidence waves. The proposed RA antenna can achieve LP, RHCP, and LHCP modes by simply rotating the reflective panel mechanically, maintaining high gain, wide 3-dB AR, and 3-dB gain bandwidths.

II. Unit Cell

The geometries of the proposed UC are shown in Fig. 1, where it consists of an air-perforated dielectric stub and a metal plate. The electromagnetic properties of the dielectric stub are with a dielectric constant of 2.65 and a loss tangent of 0.01 in the Ka-band. Since one end of the proposed UC is shorted with a metal plate, most of the electromagnetic waves will be reflected for TE and TM incidence waves, resulting in approximate full reflectance. However, the reflection phases at the interface of the air-perforated dielectric stub and air space are discriminated against for TE and TM incidence waves due to the structural asymmetry of the UC. To analyze the reflection phase of the proposed UC, equivalent dielectric constants ε_x and ε_y are introduced, where ε_x and ε_y represent the dielectric constant of

Manuscript received June, 2020. This work was supported in part by AAU Young Talent Program and also in part by the InnovationsFonden project of MARS2. (*Corresponding author: Shuai Zhang*)

The authors are all with the Antennas, Propagation and Millimeter-wave Systems (APMS) Section, Department of Electronic Systems, Aalborg University, Aalborg, 9220, Denmark. (email: sz@es.aau.dk)

the proposed UC in *x*- and *y*-direction, respectively. The values of ε_x and ε_y are closely related to the dimensions of the cuboid air void which is characterized by a length of *l*, a width of *w*, and a height of *h*.

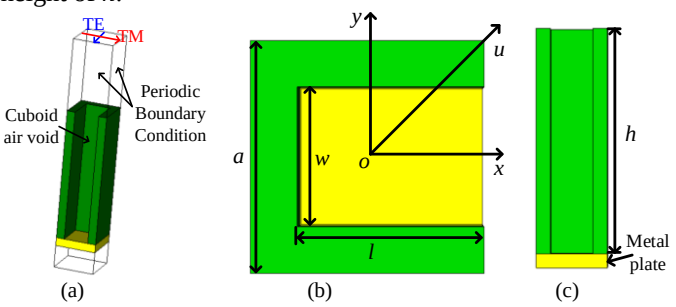

Fig. 1. The geometries of the proposed UC. (a). Perspective view. (b). Front view. (c). Side view. (*a* = 5.0 mm, *h* = 16.0 mm.)

Tab. I. A 2-bit reflection phase of the proposed UC at 30 GHz under different dimensions (*h* = 16 mm)

	l (mm)	*w* (mm)	Reflection phase
UC#1	1.9	1.55	-180 deg
UC#2	1.8	2.3	-90 deg
UC#3	1.8	3.0	0 deg
UC#4	2.0	3.5	90 deg

For the proposed UC, it can be equivalent to a transmission line to analyze its reflection phase. For a TE or TM normal incidence wave whose electric field is parallel with the *x* or *y*-axis, the reflection phases at the interface of the air-perforated dielectric stub and air space can be calculated as:

$$\theta_x = -\frac{4\pi hf}{c}\sqrt{\varepsilon_x(w,l)} + \varphi_x \quad (1a)$$

$$\theta_y = -\frac{4\pi hf}{c}\sqrt{\varepsilon_y(w,l)} + \varphi_y \quad (1b)$$

where *f* is the frequency of interest, *h* is the height of the air-perforated dielectric stub, *c* is the light speed, φ_x and φ_y are the reflection phases at the interface of the air-perforated dielectric stub and metal plate for TE and TM incidence waves, respectively.

With a specific set of *w* and *l*, the reflection phase difference for TE and TM incidence waves is given as:

$$\Delta\theta = \frac{4\pi hf}{c}\left(\sqrt{\varepsilon_y(w,l)} - \sqrt{\varepsilon_x(w,l)}\right) + \left(\varphi_x - \varphi_y\right) \quad (2)$$

The reflection phase difference for a TE or TM incidence wave with different sets of *w* and *l* can be calculated as:

$$\Delta\theta_x = \frac{4\pi hf}{c}\left(\sqrt{\varepsilon_x(w_1,l_1)} - \sqrt{\varepsilon_x(w,l)}\right) \quad (3a)$$

$$\Delta\theta_y = \frac{4\pi hf}{c}\left(\sqrt{\varepsilon_y(w_1,l_1)} - \sqrt{\varepsilon_y(w,l)}\right) \quad (3b)$$

Eqs. (3) and (4) reveal that it is possible to find out: a). a specific set of *w* and *l* to make $\Delta\theta$ equal to 90 degrees; b). some different sets of *w* and *l* to make $\Delta\theta_x$ and $\Delta\theta_y$ equal to 90 degrees. When $\Delta\theta$ equals to 90 degrees, the reflection phases in *x*- and *y*-direction would be 90-degree out of phase for a *u*-directed incidence wave, which is essential to generate circular polarization.

To simplify the implementation of the proposed RA antenna, we mainly focus on finding four sets of *w* and *l* to form four UCs, where the four UCs are required to a simultaneous 2-bit reflection phase and 90-degree out of phase for TE and TM incidence waves. Simulations and optimizations are carried out with CST Microwave Studio Software to find the desired sets of *w* and *l*, where the periodic boundary conditions (PBCs) are imposed on the UC to simulate an infinite surface. The values of *w*, *l*, and *h* should also follow the printing accuracy of our available 3D printing technology. Tab. I lists a kind of combination of *w*, *l*, and *h*.

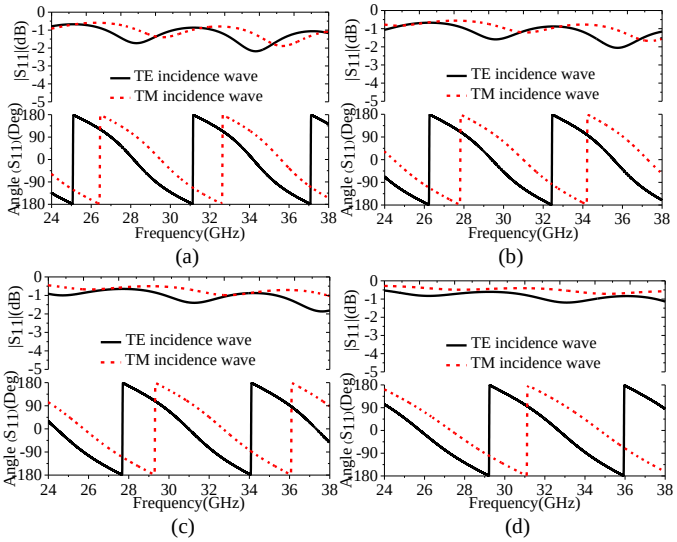

Fig. 2. The reflection amplitude and phase of the formed four UCs with TE and TM incidence waves from 24 to 38 GHz. (a). UC#1. (b). UC#2. (c). UC#3. (d). UC#4.

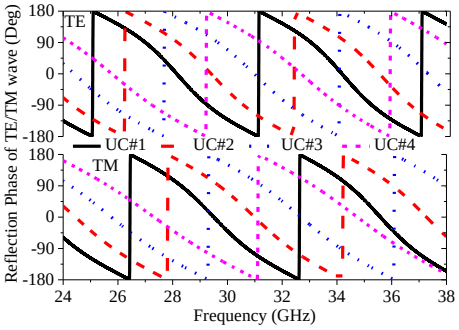

Fig. 3. The reflection phases of the formed four UCs with TE or TM normal incidence wave.

The use of dielectric material to construct the proposed UC is attributed to its wideband and minor dispersion properties. To check the wideband performance of the formed four UCs (UC#1, UC#2, UC#3, and UC#4), their reflection amplitudes and phases are simulated with TE and TM incidence waves from 24 to 38 GHz. As seen in Fig. 2, the imbalances of reflection amplitudes for all of the four UCs are less than 1 dB from 24 to 38 GHz. Besides, the phase differences for TE and TM incidence waves are around 90 deg, the imbalances of 90-degree out of phase are +/- 15 degrees.

A 2-bit reflection phase of {-π, -π/2, 0, π/2} provided by the formed four UCs are also examined for TE and TM incidence waves. Fig. 3 presents the reflection phases of the formed four

UCs, where it is observed that the four UCs can offer a 90 degrees phase gradient from 24 to 38 GHz for both TE and TM incidence waves. Even though the phase gradient between the UC#1 and UC#4 is smaller than 90 deg from 35 to 38 GHz for TM incidence wave, the smaller phase gradient would not impact its abilities for circular polarization generation. The reflection amplitudes and phases of the formed four UCs are also examined with TE and TM oblique incidence waves. It has been demonstrated from the simulated results that the reflection amplitudes and phases are still maintained when the oblique incidence angle reaches 40 degrees for both TE and TM oblique incidence waves over the entire frequency band.

III. Wideband and Polarization-Reconfigurable Reflectarray Antenna

The proposed RA antenna implemented by the formed four UCs is investigated. A RA antenna consists of a feeding source and a reflective panel with simultaneous full reflectance and phase-compensating properties. The distance between the phase center of the feeding source and reflective panel is specified as *F*, the diameter of the reflective panel is *D*. A centrally-fed method is performed to simplify the proposed RA antenna design. A linearly-polarized horn antenna operating from 22 to 40 GHz is served as the feeding source. To decrease the oblique incidence effects on the UCs, a large *F/D* ratio is preferred. However, a large *F/D* ratio would inversely lower the spillover efficiency, leading to reducing the aperture efficiency of the proposed RA antenna [24]. Here, the values of *F* and *D* are selected as 70 mm and 110 mm, respectively. Then, the reflection phase distribution on the plane of the reflective panel at 28 GHz is simulated, where the phase of every pixel ranges from - 180 to 180 degrees. However, the proposed UCs to implement the reflective panel can only offer a 2-bit reflection phase. To this end, some approximations should be taken to make the UCs feasible for the proposed RA antenna design [25]. Using the approximations, the phase distributions on the plane of the reflective panel are obtained and plotted in Fig. 4.

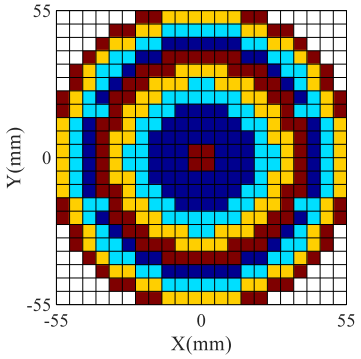

Fig. 4. The phase distribution on the plane of the reflective panel at 28 GHz. (■: π/2, ■: 0, ■: -π/2, ■: - π.)

The proposed RA antenna is then configured according to the phase distributions and the formed four UCs. The final model of the proposed RA antenna is presented in Fig. 5 (a), where the polarization of the feeding source is *x*-polarized. A 3D printed fixture is used for holding and positioning the feeding source. As introduced in Section. II, the formed four UCs are capable of converting a linearly-polarized wave to a circularly-polarized one. To this end, the proposed RA antenna can achieve different polarizations by simply rotating the 3D-printed dielectric reflective panel with the feeding source fixed, where a RHCP or LHCP mode can be obtained by rotating the reflective panel 45 and 135 degrees anti-clockwise, respectively. The corresponding RA antenna with RHCP and LHCP modes are shown in Figs. 5 (b) and (c), respectively. It should be mentioned here that the blockage effects of the centrally-fed feeding source can be minimized by using offset-fed techniques as widely reported in [26]-[28].

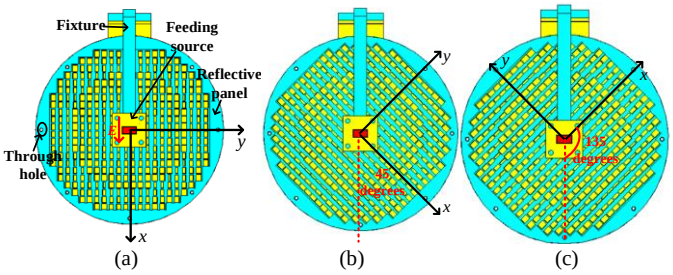

Fig. 5. The configuration of the proposed RA antenna. (a). LP mode. (b). RHCP mode. (c). LHCP mode.

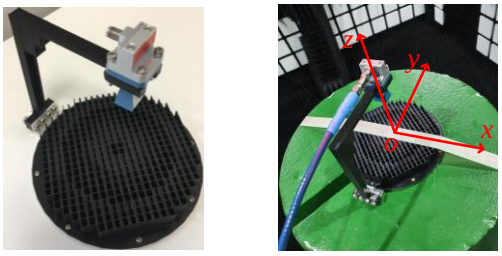

Fig. 6. The photographs of the proposed RA antenna and its measurement setup.

IV. Experimental Measurement

The proposed RA antenna has been fabricated and measured. The dielectric panel is printed with 3D printed technology and fixed to a metal plate by eight screws. The photograph of the proposed RA antenna is shown in Fig. 6

A. reflection coefficient measurement

The reflection coefficients of the proposed RA antenna with RHCP, LHCP, and LP modes are measured. For brevity, the simulated reflection coefficient with LP mode is presented for comparison. As seen in Fig. 7 (a), the measured reflection coefficients with RHCP, and LHCP, and LP modes are all below -10 dB from 24 to 38 GHz.

B. Radiation patterns and realized gain measurements

The realized gains of the proposed TA antenna with RHCP, LHCP, and LP modes are measured and compared with the simulated results. As seen in Figs. 7 (b)-(d), the measured realized gains agree very well with the simulated counterparts, where 3-dB AR bandwidths of 43.2 % and 37.5 % are obtained for RHCP and LHCP modes, respectively.

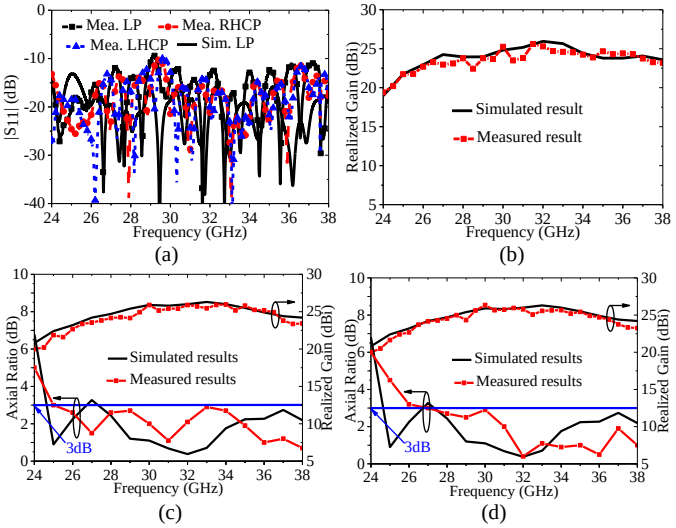

Fig. 7. The measured reflection coefficients, realized gains, and axial ratios of the proposed RA antenna with different polarization modes. (a). $|S_{11}|$. (b). LP mode. (c). RHCP mode. (d). LHCP mode.

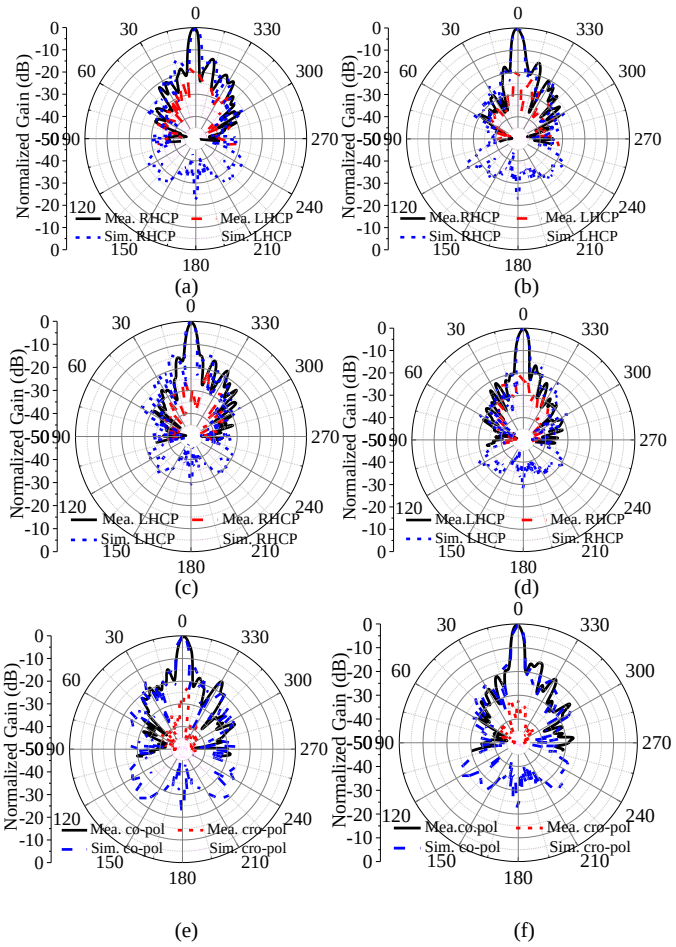

Fig. 8. The measured and simulated normalized gain of the proposed RA antenna with RHCP, LHCP, and LP modes at 30 GHz. (a). φ = 0°, RHCP mode. (b). φ = 90°, RHCP mode. (c). φ = 0°, LHCP mode. (d). φ = 90°, LHCP mode. (e). φ = 0°, LP mode. (f). φ = 90°, LP mode.

The measured 3-dB gain bandwidths of 37.5 %, 34.4 %, 37.5 %, and 1-dB gain bandwidths of 18.2 %, 18.6 %, 11.7 % are observed for RHCP, LHCP, and LP modes, respectively. According to the measured realized gains, the peak aperture efficiencies of the proposed RA antenna at 30 GHz are 32.5 %, 36 %, and 28 %, corresponding to RHCP, LHCP, and LP modes. The aperture efficiency can be further improved by using low-loss material to print the dielectric reflective panel.

The normalized gains of the proposed RA antenna with RHCP, LHCP, and LP modes are measured at 30 GHz in the cut planes of φ = 0° and φ = 90°, where the simulated results are presented for comparison. As seen in Fig. 8, the measured results agree well with the simulated ones in terms of main beam, first radiation null, and sidelobe, etc. The sidelobes and cross-polarization levels are all below -15 dB and -20 dB for RHCP, LHCP, and LP modes, respectively. It should be mentioned that the measured radiation patterns of the proposed RA antenna are all broadside and very stable from 24 to 38 GHz for RHCP, LHCP, and LP modes.

Table. II compares the proposed RA antenna with other works. The proposed RA antenna is highlighted by its high gain and wide impedance, 3-dB AR, 3-dB gain bandwidths. Compared to the polarization-reconfigurable antennas enabled by active RF components, the proposed RA antenna has advantages of simple structure and low loss. The effects of RF components on radiation patterns of antennas can be avoided. However, the proposed RA antenna suffers from a slow speed to vary its polarization compared with the ones controlled by DC bias. As a solution, a step motor can be adopted to control the rotations of reflective panel, so that the polarization can also be electrically changed in a high speed.

Tab. II. Comparisons of the proposed RA antenna with other works

Refs	-10dB Bandwidth (%)	AR Bandwidth (%)	3-dB Bandwidth (%)	Peak Gain (dBi)
[4]	8.7 (LP) 16.7(RHCP) 18.2(LHCP)	 3.2 (RHCP) 3.7 (LHCP)	N. A	10.6(LP) 10.2(RHCP) 9.8(LHCP)
[5]	14.8(LP) 29.6(RHCP) 29.6(LHCP)	 15.4(RHCP) 15.4(RHCP)	N. A	7.0(LP) 6.2(RHCP) 6.2(LHCP)
[13]	10.8 (LP) 18(RHCP) 18 (LHCP)	 15.0 (RHCP) 14.5 (LHCP)	19.2 (LP) 24 (RHCP) 23.5(LHCP)	14.7(LP) 14.0(RHCP) 14.2(LHCP)
Proposed	**> 37.5**	**43.2 (RHCP)** **37.5 (LHCP)**	**37.5 (LP)** **37.5(RHCP)** **34.4(LHCP)**	**25.3(LP)** **26.0(RHCP)** **25.8(LHCP)**

V. Conclusion

This letter has described a wideband and polarization-reconfigurable millimeter-wave reflectarray (RA) antenna. By simply rotating the reflective panel, the proposed RA antenna can work as a LP, RHCP, or LHCP antenna. The measured 3-dB axial ratio bandwidths for RHCP and LHCP modes are 43.2 % and 37.5 %, respectively. The 3-dB gain bandwidths for RHCP, LHCP, and LP modes are 37.5 %, 34.4 %, and 37.5 %, respectively. Due to the low-cost, high-gain, wideband, and wide 3-dB axial ratio properties, the proposed RA antenna is an attractive candidate for 5G millimeter-wave communication systems.

REFERENCES

[1] F. Ferrero, C. Luxey, G. Jacquemod, and R. Staraj, "Dual-band circularly polarized microstrip antenna for satellite," *IEEE Antennas Wireless Propag Lett.*, vol. 4, pp. 13-15, 2005.

[2] E. Kaivanto, M. Berg, E. Salonen, and P. Maagt, "Wearable circularly polarized antenna for personal satellite communication," *IEEE Trans. Antennas Propag*., vol. 59, no. 12, pp. 4490-4496, Dec. 2011.

[3] H. Aissat, L. Cirio, M. Grzeskowiak, J. Laheurte, and O. Picon, "Reconfigurable circularly polarized antenna for short-range communication systems," *IEEE Trans. Microw, Theory Techn*., vol. 54, no. 6, pp. 2856-2863, Jun. 2006.

[4] Q. Chen, J. Li, G. Yang, B. Cao, and Z. Zhang, "A polarization-reconfigurable high-gain microstrip antenna," *IEEE Trans. Antennas Propag*., vol. 67, no. 5, pp. 3461-3466, May. 2019.

[5] H. Tran, and H. Park, "Wideband reconfigurable antenna with simple biasing circuit and tri-polarization diversity," *IEEE Antennas Wireless Propag. Lett.*, vol. 18, no. 10, pp. 2001- 2005, Oct. 2019.

[6] Y. Sung, T. Jang, and Y. Sim, "A reconfigurable microstrip antenna for switchable polarization," *IEEE Microw. Wireless Compon. Lett*., vol. 14, no. 11, pp. 534-536, Nov. 2004.

[7] A. Khidre, K. Lee, F. Yang, and A. Elsherbeni, "Circular polarization reconfigurable wideband E-shaped patch antenna for wireless applications," *IEEE Trans. Antennas Propag*., vol. 61, no. 2, pp. 960-964, Feb. 2013.

[8] B. Kim, B. Pan, S. Nikolaou, Y. Kim, J. Papapolymerou, and M. Tentzeris, "A novel single-feed circular mictrostrip antenna with reconfigurable polarization capability," *IEEE Trans. Antennas Propag*., vol. 56, no. 3, pp. 630-638, Mar. 2008.

[9] D. Seo, J. Kim, M. Tentzeris, and W. Lee, "A quadruple-polarization reconfigurable feeding network for UAV RF sensing antenna," *IEEE Microw. Wireless Compon. Lett*., vol. 29, no. 3, pp. 183-185, Mar. 2019.

[10] H. Sun, and S. Sun, "A novel reconfigurable feeding network for quad-polarization-agile antenna design," *IEEE Trans. Antennas Propag*., vol. 64, no. 1, pp. 311-316, Jan. 2016.

[11] S. Lee, and Y. Sung, "Simple polarization-reconfigurable antenna with T-shaped feed," *IEEE Antennas Wireless Propag. Lett*., vol. 15, pp. 114-117, 2016.

[12] H. Sun, and Z. Pan, "Design of a quad-polarization-agile antenna using a switchable impedance converter," *IEEE Antennas Wireless Propag. Lett*., vol. 18, no. 2, pp. 269-273, Feb. 2019.

[13] N. Zhu, X. Yang, T. Lou, Q. Cao, and S. Gao, "Broadband polarization-reconfigurable slot antenna and array with compact feed network," *IEEE Antennas Wireless Propag. Lett*., vol. 18, no. 6, pp. 1293-1297, June. 2019.

[14] E. Abbas, N. Nguyen-Trong, A. Mobashsher, and A. Abbosh, "Polarization-reconfigurable antenna array for millimeter-wave 5G," *IEEE Access*, vol. 7, pp.131214-131220, Sep. 2019.

[15] H. Zhu, S. Cheung, X. Liu, and T. Yuk, "Design of polarization reconfigurable antenna using metasurface," *IEEE Trans. Antennas Propag*., vol. 62, no. 6, pp. 2891-2898, June. 2014.

[16] I. McMichael, "A mechanically reconfigurable patch antenna with polarization diversity," *IEEE Antennas Wireless Propag. Lett*., vol. 17, no. 7, pp. 1186-1189, July. 2018.

[17] P. Mei, S. Zhang, and G. Pedersen, "A low-cost, high-efficiency and full-metal reflectarray antenna with mechanically 2-D beam-steerable capabilities for 5G application," *IEEE Trans. Antennas Propag*., Early access.

[18] T. Debogovic, and J. Perruisseau-Carrier, "Low loss MEMS-reconfigurable 1-bit reflectarray cell with dual-linear polarization," *IEEE Trans. Antennas Propag*., vol. 62, no.10, pp. 5055-5060, Oct. 2014.

[19] S. Hum, and J. Perruisseau-Carrier, "Reconfigurable reflectarrays and array lens for dynamic antenna beam control: A review," *IEEE Trans. Antennas Propag*., vol. 62, no.1, pp. 183-198, Jan. 2014.

[20] H. Yi, S. Qu, K. Ng, C. Chan, and X. Bai, "3-D printed millimeter-wave and terahertz lenses with fixed and frequency scanned beam," *IEEE Trans. Antennas Propag*., vol. 64, no.2, pp. 442-449, Feb. 2016.

[21] P. Mei, S. Zhang, X. Lin, and G. Pedersen, "A millimeter-wave gain-filtering transmitarray antenna design using a hybrid lens," *IEEE Antennas Wireless Propag. Lett*., vol. 18, no. 7, pp. 1362-1366, July. 2019.

[22] P. Nayeri, M. Liang, R. A. Sabory-Garcia, M. Tuo, F. Yang, H. Xin, and A. Elsherbeni, "3D printed dielectric reflectarrays: low-cost high gain antennas at sub-millimeter waves," *IEEE Trans, Antennas Propag*., vol. 62, no. 4, pp. 2000-2008, Apr 2014.

[23] K. Wang, and H. Wong, "A wideband millimeter-wave circularly polarized antenna with 3-D printed polarizer," *IEEE Trans, Antennas Propag*., vol. 65, no. 3, pp. 1038-1046, Mar. 2017.

[24] A. Yu, F. Yang, A. Elsherbeni, J. Huang, and Y. Rahamt-Samii, "Aperture efficiency analysis of reflectarray antennas," *Microw. Opt. Technol Lett*., vol. 52, no. 3, pp. 771-779, Mar. 2004.

[25] Y. Ge, C. Lin, and Y. Liu, "Broadband folded transmitarray antenna based on an ultrathin transmission polarizer," *IEEE Trans. Antennas Propag*., vol. 66, no. 11, pp. 5974-5981, Aug. 2018.

[26] P. Mei, S. Zhang, Y. Cai, X. Q. Lin, and G. F. Pedersen, "A reflectarray antenna designed with gain filtering and low-RCS properties," *IEEE Trans, Antennas Propag*., vol. 67, no. 8, pp. 5362-5371, Aug 2019.

[27] P. Nayeri, M. Liang, R. A. Sabory-Garcia, M. Tuo, F. Yang, H. Xin, and A. Elsherbeni, "3D printed dielectric reflectarrays: low-cost high gain antennas at sub-millimeter waves," *IEEE Trans, Antennas Propag*., vol. 62, no. 4, pp. 2000-2008, Apr 2014.

[28] R. Deng, Y. Mao, S. Xu, and F. Yang, "A single-layer dual-band circularly polarized reflectarray with high aperture efficiency," *IEEE Trans, Antennas Propag*., vol. 63, no. 7, pp. 3317-3320, July 2015.